 https://doi.org/10.3311/PPci.40684

Periodica Polytechnica Civil Engineering, 69(4), pp. 1108–1123, 2025

Numerical Investigation of Wave Induced Scour Depth Around Slender and Grouped Monopile

Bekir Sürücü[1], Deniz Bayraktar Bural[1*]

[1] Department of Shipbuilding and Ocean Engineering, Faculty of Naval Architecture and Ocean Engineering, Istanbul Technical University, 34469 Maslak/Istanbul, Turkiye
[*] Corresponding author, e-mail: bayraktard@itu.edu.tr

Received: 11 April 2025, Accepted: 17 August 2025, Published online: 06 September 2025

Abstract

Wave-induced scour around monopile foundations poses a critical challenge for offshore wind turbine design, affecting stability, serviceability, and maintenance costs. Despite extensive experimental studies, high-fidelity numerical tools are still needed to capture complex interactions between wave kinematics, sediment transport, and pile geometry. This study presents a numerical investigation of scour depth around slender monopiles under regular wave conditions. A validated three-dimensional CFD model (FLOW-3D) employing the Volume of Fluid method and RNG k–ε turbulence closure was used to simulate wave–structure–seabed interaction. Sediment transport was modeled using the Meyer–Peter and Müller bedload formulation and an advection–diffusion equation for suspended load. The influence of the Keulegan–Carpenter (KC) number was examined for KC = 8.8–24, covering inertia- and drag-dominated regimes. Results showed that higher KC values intensified vortex-induced sediment transport and scour, while lower KC values led to gradual development. A marked increase occurred beyond KC ≈ 14, indicating a regime shift in flow–sediment interaction. Grouped-cylinder cases at G/D = 1 and 2 showed that narrow spacing produced mutual sheltering and reduced scour, whereas wider spacing caused deeper localized erosion. Single monopile predictions matched experimental data and empirical formulas, demonstrating the model's predictive capability. These findings emphasize the strong KC dependence of scour and suggest that spacing ratios above G/D = 1.5 may help mitigate adverse group effects in array layouts under oscillatory wave forcing.

Keywords

sediment transport, scour depth, wave, offshore pile

1 Introduction

Monopile foundations have gained prominence in offshore engineering, particularly with the global expansion of offshore wind energy. While monopiles offer structural simplicity and ease of installation, their interaction with marine environments introduces notable engineering challenges. In particular, slender monopiles – those with diameters significantly smaller than the incident wavelength – can experience flow regimes dominated either by inertia or drag, depending on the Keulegan–Carpenter (KC) number. As the KC number increases, drag forces become more influential, altering the flow behavior around the monopile and contributing to vortex shedding, sediment transport, and ultimately, scour formation.

Scour is a serious concern for offshore foundations, as it may compromise structural stability and lead to increased fatigue or even failure in extreme conditions [1, 2]. This makes it essential to understand and predict scour behavior accurately, especially as offshore wind projects are developed in deeper and more energetic waters. Although extensive research has been conducted on scour around marine structures such as pipelines and bridge piers [3–5], studies focusing specifically on monopiles under wave action remain limited. However, several recent studies have contributed valuable insights into monopile scour under wave conditions. Ye et al. [6] experimentally examined the coupled response of monopiles, seabed, and waves under varying sea conditions, while Guo and Lo [7] numerically investigated wave interaction with cylinders over mud beds. Xu and Huang [8] addressed the effects of solitary-wave-induced scour and pile spacing experimentally. Additionally, Zhang et al. [9] and Ma et al. [10] employed CFD–DEM coupling methods to simulate

Cite this article as: Sürücü, B., Bayraktar Bural, D. "Numerical Investigation of Wave Induced Scour Depth Around Slender and Grouped Monopile", Periodica Polytechnica Civil Engineering, 69(4), pp. 1108–1123, 2025. https://doi.org/10.3311/PPci.40684

and validate local scour development around monopiles, demonstrating the advantages of hybrid numerical techniques in capturing complex sediment dynamics.

The mechanics of scour around cylindrical structures have long been of interest. Seminal studies by Sumer et al. [11] and Whitehouse [12] examined the influence of pile diameter, water depth, and wave parameters, and emphasized the importance of horseshoe and lee-wake vortices in the development of scour. Later, Melville and Coleman [13] and Sumer and Fredsøe [14] advanced this understanding by exploring the interactions between hydrodynamic forces and seabed erosion. More recently, Fowai et al. [15] evaluated the performance of offshore wind turbine (OWT) foundations, noting how foundation type can influence preliminary design. While the present study does not investigate structural countermeasures, previous work has shown that modifications such as collars may reduce local scour [16].

Scour timescales have also been studied extensively in recent years, particularly in connection with the KC number. Petersen et al. [17] introduced design tools that account for the combined effects of waves and currents. Zhang et al. [18] conducted detailed experiments on the dynamic characteristics of monopile foundations under local scour induced by combined wave and current interactions, emphasizing the increase in scour depth and structural response under such conditions.

Sumer et al. [19] proposed empirical expressions to predict backfilling times in various flow conditions. Chen and Li [20] developed a formulation suited for steady current conditions but adaptable to wave scenarios. Later, Chen et al. [21] emphasized the role of scaling laws in predicting scour depth and time evolution, while Larsen and Fuhrman [22] offered a new empirical expression for equilibrium scour and timescales. Although some recent studies have addressed time-dependent scour behavior under unsteady flow conditions, such as those on bridge piers exposed to flood hydrographs [23], research remains limited for monopiles subjected to wave-dominated environments. These contributions underscore the ongoing need for models that perform reliably under a wide range of marine conditions.

Computational Fluid Dynamics (CFD) has become an essential tool for examining these complex interactions in detail. CFD enables three-dimensional modeling of fluid and sediment dynamics around monopiles, providing insights that complement or extend beyond physical experiments [24, 25]. Despite its advantages, CFD-based prediction of scour remains challenging, particularly at low KC numbers where inertial effects dominate and flow displacement per wave cycle is limited [20]. This limitation often results in discrepancies between numerical and experimental findings. For instance, Zhao et al. [26] developed a finite element approach to simulate wave-induced scour, accounting for wave diffraction and steady streaming effects, and showing how KC and sediment properties affect scour progression.

Building on such studies, the present research employs a three-dimensional CFD model based on the Navier–Stokes equations and a Volume of Fluid (VOF) method to simulate the coupled interaction of waves, flow, and sediment transport around slender monopiles. In addition to examining scour under various KC regimes, this study also investigates the effect of monopile grouping – an area with limited existing research – by analyzing different pile spacing ratios. By validating the CFD model with experimental data from Sumer et al. [11], the study explores how KC number and Shields parameter influence scour depth and timescales in wave environments. The findings aim to contribute to both fundamental understanding and practical design guidance for offshore wind turbine foundations.

While previous studies have primarily addressed wave-induced scour around single monopiles, often within a limited range of flow conditions, this study aims to complement the existing literature by applying a validated CFD model across varying KC regimes, including both drag- and inertia-dominated cases. Additionally, the effect of monopile grouping – less frequently explored in wave-only conditions – is examined through simulations at two different spacing ratios. Although the modeling techniques are based on established methods, the structured application across multiple configurations and the direct comparison with experimental and empirical results provide additional insight into scour behavior. The study is intended to support preliminary design considerations by clarifying how pile arrangement and flow regime interact to influence seabed response.

The selected KC values (8.8, 14.6, and 24) were derived by adjusting the flow velocity while keeping the wave period (T = 4.5 s) and monopile diameter (D = 0.1 m) constant. KC served as the primary hydrodynamic control parameter to examine regime-dependent scour behavior around single monopiles. For the grouped monopile cases, a representative KC = 13 condition was selected to isolate the effects of pile spacing under controlled wave forcing. This setup captures flow–sediment interaction scenarios relevant to shallow-water monopile foundations.

2 Methods

The numerical simulations in this study were conducted using FLOW-3D®, which offers specialized modules for free-surface flow, sediment transport, and wave–structure interaction modeling. The model solves the incompressible Navier–Stokes and continuity equations using the Volume of Fluid (VOF) method to track the air–water interface. Turbulent flow was modeled using the Renormalization Group (RNG) k–ε turbulence model, which is suitable for capturing complex near-wall flow structures around cylindrical bodies.

Sediment transport and scour development were simulated by implementing the Meyer–Peter and Müller bedload transport formula. The Shields parameter (θ) was used to determine the initiation of sediment motion, with transport triggered once the local shear stress exceeded a critical threshold (θ_{cr}). In each computational cell, hydrodynamic forces acting on sediment particles – including bed shear stress and drag – were evaluated to model both suspended load and bedload transport.

The computational domain was discretized using a structured mesh, with local refinement in the vicinity of the monopile to resolve near-bed velocity gradients and vortex structures. Key flow parameters such as the Keulegan–Carpenter number (KC) and the Shields parameter were used to characterize flow regimes and sediment mobility. Simulations were conducted for KC numbers greater than or equal to 6, focusing on drag-dominated conditions typical of slender monopiles in wave environments.

Model performance was assessed by comparing numerical predictions to experimental results reported by Sumer et al. [11] and Larsen and Fuhrman [22]. Both the equilibrium scour depth and the non-dimensional time scale T^* were evaluated to verify the accuracy of the simulations in capturing scour progression over time.

This methodology provides a robust framework for simulating wave-induced scour and sediment transport around slender monopiles, with particular emphasis on the role of hydrodynamic parameters in controlling scour dynamics.

2.1 Numerical model

The numerical analysis was conducted using a CFD model that solves the incompressible Navier–Stokes and continuity equations over a structured mesh domain surrounding the monopile. Wave–structure interaction at the air–water interface was modeled using the Volume of Fluid (VOF) method, which is widely applied for capturing free surface dynamics under wave action. To represent the monopile geometry within the computational domain, the Fractional Area–Volume Obstacle Representation (FAVOR) method [27] was employed. The combination of VOF and FAVOR, together with porosity-based functions, enabled detailed modeling of near-field fluid–structure interaction.Turbulence effects were simulated using the Renormalization Group (RNG) k–ε model, which is suitable for capturing separated and recirculating flow patterns around cylindrical bodies. Sediment transport was modeled through the Meyer–Peter and Müller formulation for bedload, with sediment motion triggered when the Shields parameter exceeded a critical threshold. Mesh refinement was applied near the monopile to resolve near-bed velocity gradients and sediment transport more accurately. This localized refinement contributed to improved prediction of flow behavior and scour development around the structure.

2.1.1 Governing equations

The numerical model is based on the conservation of mass and momentum for incompressible fluid flow. These governing equations form the foundation of computational fluid dynamics (CFD) and consist of the continuity equation:

$$\frac{\partial u_i}{\partial x_i} = 0\,, \tag{1}$$

where u_i is the velocity component and x_i is the spatial coordinate.

The incompressible Navier–Stokes equations are expressed as:

$$\frac{\partial u_i}{\partial t} + u_j \frac{\partial u_i}{\partial x_j} = -\frac{1}{\rho}\frac{\partial P}{\partial x_j} + \frac{\partial}{\partial x_j}\left(2\nu S_{ij} - \overline{u_i' u_j'}\right), \tag{2}$$

here, P is the pressure, ρ is the fluid density, ν is the kinematic viscosity, and $\overline{u_i' u_j'}$ represents the Reynolds stress tensor. The strain rate tensor S_{ij} which characterizes the deformation rate of fluid elements, is defined as:

$$S_{ij} = \frac{1}{2}\left(\frac{\partial u_i}{\partial x_j} + \frac{\partial u_j}{\partial x_i}\right) \tag{3}$$

The Reynolds stresses are modeled using the eddy viscosity concept:

$$\overline{u_i' u_j'} = \nu_t\left(\frac{\partial u_i}{\partial x_j} + \frac{\partial u_j}{\partial x_i}\right) - \frac{2}{3}k\delta_{ij} \tag{4}$$

In Eq. (4), ν_t is the turbulent (eddy) viscosity, k is the turbulent kinetic energy, and δ_{ij} is the Kronecker delta, defined as $\delta_{ij} = 1$ when $i = j$ and $\delta_{ij} = 0$ otherwise.

All equations were discretized using the finite volume method, which ensures local conservation and is well suited for complex boundaries such as wave–structure interactions [28].

2.1.2 Turbulence model

Turbulence was modeled using the Renormalization Group (RNG) k–ε formulation, which provides a balance between accuracy and computational efficiency. This model is an enhanced version of the standard k–ε approach and incorporates statistical renormalization to better capture small-scale turbulence effects, especially in regions with high strain rates or rapidly changing flow fields [29].

These features are particularly relevant for wave–structure interactions, where flow separation and vortex shedding around the monopile generate localized turbulent structures. Compared to more advanced models such as Large Eddy Simulation (LES), the RNG model offers reasonable accuracy with significantly reduced computational cost [30].

Additionally, the RNG k–ε model includes modifications that improve its ability to simulate flow separation, recirculation zones, and streamline curvature–conditions frequently encountered around monopiles under wave loading. This enhanced capability contributes to more realistic turbulence representation and improves the prediction of scour depth.

Near-wall treatment in the RNG k–ε model was implemented using standard wall functions. This method enables efficient estimation of bed shear stress by avoiding the need to fully resolve the viscous sublayer, while still capturing the essential dynamics of sediment mobilization near the seabed. This choice is consistent with previous scour studies where RNG k–ε yielded reliable results [9]. While more advanced models like LES could offer finer resolution of turbulent structures, RNG k–ε offers a practical balance between accuracy and computational cost for engineering-scale scour simulations.

2.1.3 Sediment and bed load transport model

Accurate modeling of sediment transport is essential for predicting scour development around the monopile. In this study, transport processes were represented using empirical and theoretical formulations that relate sediment motion to local hydrodynamic conditions.

Bed shear stress and drag forces were evaluated in each computational cell. Sediment motion was initiated when the dimensionless Shields parameter θ exceeded a critical value θ_{cr}. The bedload transport rate was calculated using the Meyer–Peter and Müller formula:

$$\Phi = \beta\left(\theta - \theta_{cr}\right), \tag{5}$$

where Φ is the dimensionless transport rate and β is an empirical coefficient that varies depending on the intensity of transport. The value of β is an empirical coefficient, assumed to be 8 in this study for moderate transport conditions.

The corresponding volumetric sediment transport rate q_b can be written as:

$$q_b = \Phi\left[g\frac{\rho_s - \rho}{\rho}d_s^3\right]^{1/2}, \tag{6}$$

where g is the acceleration due to gravity, ρ_s is the density of the sediment, ρ is the fluid density, and d_s is the sediment particle diameter. Sediment properties such as grain size, density, critical shear stress, and angle of repose were incorporated as input parameters [31].

Suspended sediment transport was modeled using the advection–diffusion equation:

$$\frac{\partial C_s}{\partial t} + \nabla\cdot\left(uC_s\right) = \text{Diffusion}, \tag{7}$$

where C_s is the sediment concentration and u is the local fluid velocity.

In this study, the critical Shields parameter θ_{cr} was set to 0.047, consistent with the sediment properties and flow regime modeled. This value of $\theta_{cr,i}$ was specified as a user-defined input, ensuring accurate representation of the threshold shear stress required to initiate sediment motion. The direct specification of θ_{cr} allowed for calibration of the model against expected transport conditions, providing a robust foundation for the prediction of scour depth and sediment displacement around the monopile.

2.1.4 Scour depths

Scour depth predictions were based on simulations conducted for Keulegan–Carpenter (KC) numbers equal to or greater than 6, where flow becomes increasingly influenced by vortex formation and sediment mobilization. Under such conditions, the equilibrium scour depth was estimated using the empirical expression:

$$\frac{S}{D} = 1.3\left\{1 - \exp\left[-0.03\left(KC - 6\right)\right]\right\}; \quad KC \geq 6 \tag{8}$$

This equation predicts the relative scour depth S/D as a function of the KC number and is widely adopted in wave-induced scour assessments. The simulation results confirmed that scour depth increases with KC, consistent with the growing influence of wave-induced vortices.

For higher KC values, particularly around slender monopiles, the flow becomes drag-dominated, resulting in enhanced vortex structures such as horseshoe and wake vortices. These features significantly contribute to sediment entrainment and deeper scour at the monopile base. Although detailed flow structures were not directly visualized, the resulting scour patterns align with trends reported in earlier experimental and numerical studies.

Previous research by Sumer and Fredsøe [14], among others, emphasized the importance of KC in governing scour development. The present results support these findings and demonstrate the reliability of the empirical approach in capturing key aspects of wave-induced scour behavior.

2.2. Mesh convergence study

To ensure the accuracy of wave generation in the numerical model, a preliminary simulation was performed using an open domain without any structural elements. This setup was used to validate the model's ability to replicate key wave characteristics – namely wave height, period, and wavelength – in accordance with theoretical expectations based on linear wave theory.

A grid convergence study was conducted by testing several spatial resolutions: 0.05 m, 0.04 m, 0.03 m, and 0.02 m. The resulting free surface elevations from each simulation were compared against theoretical predictions. As illustrated in Fig. 1, finer grid resolutions led to improved agreement with the expected wave profile.

Among the tested configurations, the grid size of 0.02 m produced the most accurate results, closely matching the theoretical wave behavior and providing a smooth, well-resolved free surface. Based on this outcome, the 0.02 m resolution was selected for all subsequent simulations involving wave–structure interactions. This grid size was applied uniformly across the entire computational domain without any local refinement, as illustrated in Fig. 2. Using this uniform grid and the known model dimensions, the total number of cells in the final mesh was approximately 2.1 million.

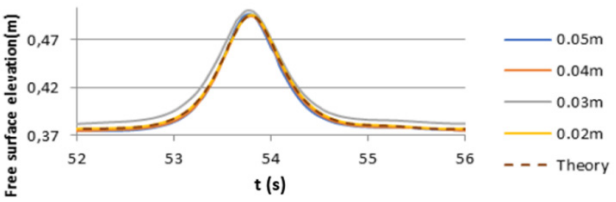

Fig. 1 Grid convergence study

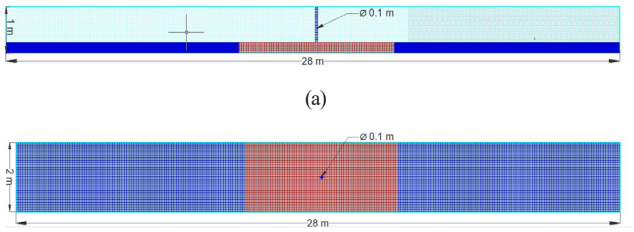

Fig. 2 Numerical model setup showing mesh distribution: (a) numerical model profile view, (b) top view of the numerical model

This mesh convergence validation is a critical step, as it confirms the model's capacity to accurately simulate wave propagation in a controlled environment. Establishing this accuracy provides a strong foundation for confidence in the results of more complex simulations, such as those involving monopile-induced scour.

2.3 Numerical model setup

To replicate the conditions observed in the experimental study by Sumer et al. [11], a numerical model was constructed with careful attention to geometric fidelity and physical parameters. The model configuration was designed to closely match the laboratory setup, ensuring consistency in wave conditions, structural placement, and sediment properties. Figs. 3(a) and 3(b) present the top and

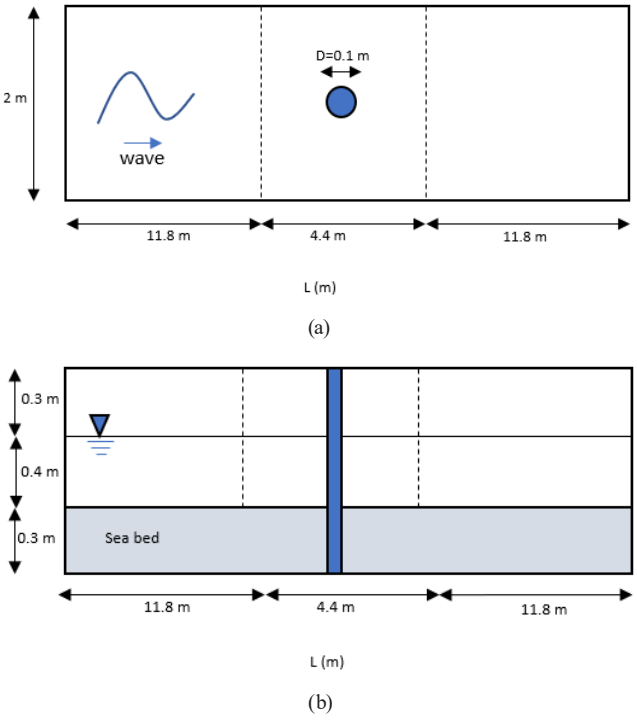

Fig. 3 The experimental set-up by Sumer et al. [11]: (a) top view, (b) side view

side views of the experimental arrangement, respectively, serving as visual references for the spatial domain.

The simulation was carried out for a duration of 3600 sec, with emphasis on accurately modeling sediment scour, turbulence behavior, and mesh resolution. The RNG k–ε turbulence model was employed, as it is widely recommended in the literature for simulations involving wave–structure interactions. Its ability to represent turbulent flow in the vicinity of cylindrical structures makes it particularly well-suited for modeling scour around monopiles.

Figs. 2(a) and 2(b) show the profile and top views of the developed numerical model, highlighting the computational mesh distribution. The simulation domain dimensions were set to 28.0 m in length, 2.0 m in width, and 1.0 m in height. A monopile with diameter D = 0.10 m was placed at the domain center, consistent with the experimental configuration. To minimize artificial wave reflections, a wave absorber was incorporated at the end of the domain. The final mesh consisted of a uniform grid with a cell size of 0.02 m throughout the entire computational domain, as illustrated in Fig. 2.

The boundary conditions and fluid domain configuration are shown in Figs. 4(a) and 4(b), including the applied water level and placement of the wave absorber. Specifically, the inlet boundary was defined as a velocity inlet using FLOW-3D's wave generation module to simulate regular wave forcing. This module prescribes orbital velocity profiles based on linear wave theory to accurately represent wave-induced flow. The outlet was treated as a pressure outlet to enable wave transmission and minimize reflection. The top boundary was set as a free-slip surface to represent the air–water interface. The bottom boundary was modeled as a no-slip wall with sediment transport enabled to capture scour development. Near-wall flow was treated using standard wall functions within the RNG k–ε turbulence model, enabling accurate estimation of bed shear stresses critical for sediment mobilization and scour evolution.Sediment transport is governed by local bed shear stresses and critical Shields parameter, enabling dynamic bed morphology evolution. The side boundaries were defined as symmetry planes to reduce lateral constraints on the flow while maintaining numerical stability. These symmetry planes allow the assumption of lateral flow uniformity and reduce computational cost. A wave absorber zone was implemented near the downstream end to attenuate reflected wave energy and ensure accurate wave–structure interaction. The absorber works by gradually increasing numerical damping in the absorption zone to minimize wave reflections. The computational domain was initialized with a quiescent water surface and a uniform sediment layer. A short pre-run period was used to stabilize the hydrostatic pressure field and sediment bed before the start of wave generation. Model accuracy was evaluated by comparing the numerical predictions of scour depth and time-dependent scour evolution with the experimental results of Sumer et al. [11].

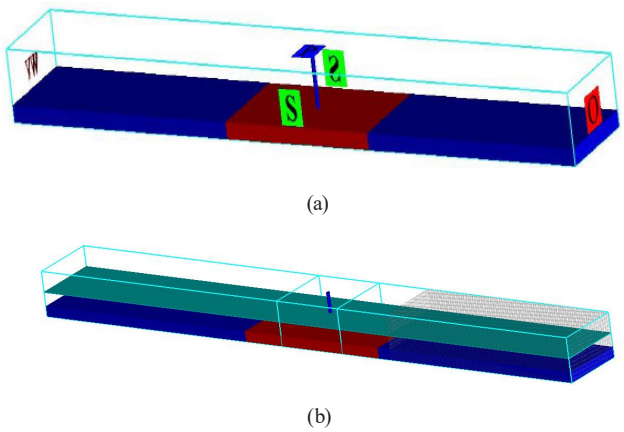

(a)

(b)

Fig. 4 Boundary conditions and numerical model configuration: (a) boundary conditions of numerical model, (b) numerical model with fluid elevation and wave absorber

Additionally, the simulation outcomes were compared with the empirical formulations provided by Larsen and Fuhrman [22], who re-parameterized equilibrium scour depths and time scales for monopiles under various hydrodynamic conditions.

3 Results

This section presents the results of numerical simulations conducted to analyze wave-induced scour around a monopile, with particular focus on the influence of different Keulegan–Carpenter (KC) numbers.

Table 1 summarizes the key parameters and results for the three test cases examined in the study. The parameters include the KC number, wave period (T), wave height (H_w), maximum orbital velocity (U_m), and the Shields parameter (θ). For each case, the dimensionless time scale (T^*) and the dimensionless scour depth (S/D) are provided, based on experimental data from Sumer et al. [11], the empirical formulation given in Eq. (8), and the present numerical simulation results. The dimensionless time scale T^*, defined in Eq. (9), is used to normalize simulation duration relative to wave period and monopile diameter, allowing cross-comparison among cases. The final numerical scour depth (S/D) values were extracted from the simulation results at the end of each run. Specifically, Figs. 5–7 correspond to the final scour state for Cases 1, 2, and 3, respectively, and serve as the basis for the numerical S/D values reported in Table 1.

Table 1 Summary of simulation parameters, Dimensionless Time Scales (T^*) and Scour Depth (S/D) results for different KC numbers

Case	KC	Wave Period (T)	Wave Height (H_w)	Orbital Velocity (U_m)	Shields Parameter (θ)	Dimensionless Time (T^*)	S/D Experiment by Sumer et al. [11]	S/D Emprical (Eq. (8))	S/D (Numerical)
Case 1	8.8	2.2 s	0.17 m	0.39 m/s	0.14	0.25	0.057	0.10	0.052
Case 2	14.6	4.5 s	0.12 m	0.33 m/s	0.13	1.42	0.22	0.29	0.25
Case 3	24	4.5 s	0.22 m	0.53 m/s	0.22	1.30	0.31	0.54	0.30

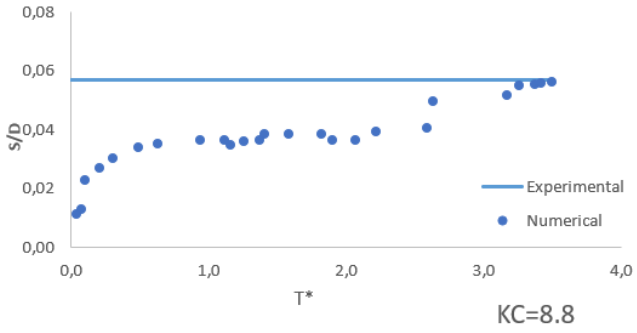

Fig. 5 Time development of scour depth from the numerical model for Case 1 (KC = 8.8), compared to the final equilibrium scour depth from experimental data by Sumer et al. [11]

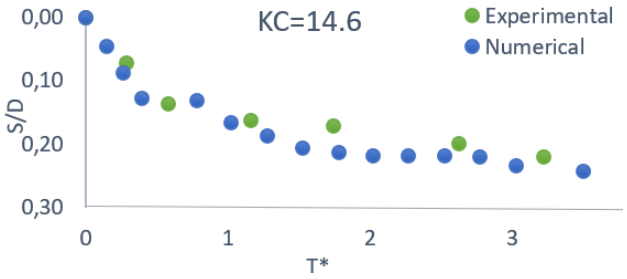

Fig. 6 Comparison of the time development of scour depth between numerical simulations and experimental data for Case 2 (KC = 14.6). The blue dots represent the experimental results from test number 46 in Sumer et al. [11].

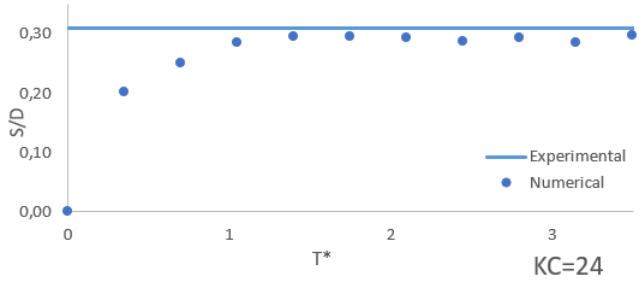

Fig. 7 Time development of scour depth from the numerical model for Case 3 (KC = 24), compared to the final equilibrium scour depth from experimental data by Sumer et al. [11]

As shown in Table 1, an increase in the KC number corresponds with an increase in the predicted scour depth across all three datasets. Case 1, which represents the lowest KC number (8.8), corresponds to the lowest scour depths, with $S/D = 0.057$ in the experiment and 0.052 in the numerical simulation. In contrast, Case 3, with a KC number of 24, shows deeper scour development, with experimental and numerical values of 0.31 and 0.30, respectively. To quantify the agreement between the numerical model and experimental data, a percentage error analysis was conducted based on the final scour depth (S/D) values in Table 1. The numerical model underpredicts the experimental scour depth by approximately 8.8% for Case 1, overpredicts by 13.6% in Case 2, and slightly underpredicts by 3.2% in Case 3. The empirical results slightly overpredict the scour depth in all three cases, particularly for the higher KC scenarios, which is consistent with findings in the literature that note the empirical model's tendency to estimate upper-bound scour depths.

The results indicate good agreement between the numerical predictions and the experimental observations, particularly in Cases 2 and 3. The slight underprediction in Case 1 may be attributed to challenges in simulating the early stages of scour development at low KC values, where the flow is less energetic and vortex-induced transport is weaker. Overall, the consistency between the numerical and experimental results validates the model's capacity to reproduce wave-induced scour behavior across a range of flow regimes.

3.1 Scour depth around single monopile

Each simulation was designed to closely replicate the experimental conditions in order to assess the numerical model's ability to predict the temporal development of wave-induced scour. The computed results were validated against the experimental data reported by Sumer et al. [11] and compared with empirical predictions to evaluate model accuracy. Figs. 8–12 are included to qualitatively illustrate the spatial patterns and progressive development of scour under wave forcing. Although these figures are not directly tied to specific KC cases, they help convey the general flow behavior and scour asymmetry observed in the simulations. Their role is primarily illustrative, intended to offer physical context rather than serve as the basis for numerical analysis.

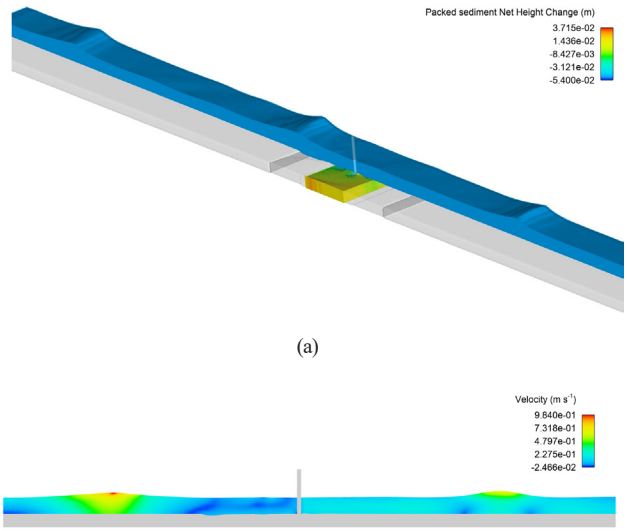

(a)

(b)

Fig. 8 Numerical model domain illustrating wave-induced scour around the monopile: (a) isometric view of the numerical model domain showing the monopile and surrounding bed surface among waves, (b) profile view of bed profile among waves

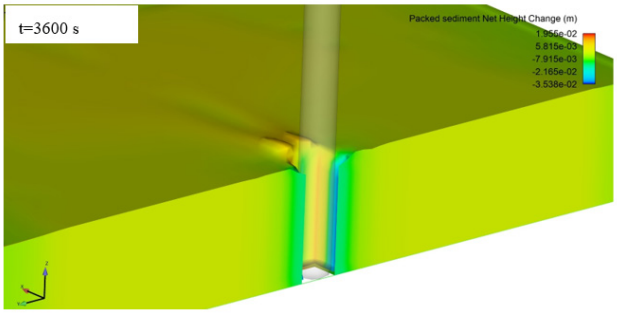

Fig. 9 Cross-sectional view of the scour around the monopile at 3600 sec, showing the extent of scour development on the sides of the pile

Fig. 8(a) illustrates an isometric view of the computational domain, showing the monopile and surrounding seabed subjected to wave forcing. The color gradient represents scour depth, with red indicating maximum erosion and blue indicating minimal seabed displacement. This visualization helps capture the spatial extent of wave-induced scour.

Fig. 8(b) presents a profile view of the wave and seabed. In this visualization, only the colored region around the pile was modeled as a scouring bed, and the color-coded scale provides an intuitive depiction of sediment displacement. This profile highlights how scour develops in the immediate vicinity of the monopile, where hydrodynamic forces are strongest.

Fig. 9 offers a cross-sectional perspective of the scour pit after 3600 sec of simulation. The scour depth distribution on the sides of the monopile and the local backfilling behind it are clearly visible. This visualization captures the

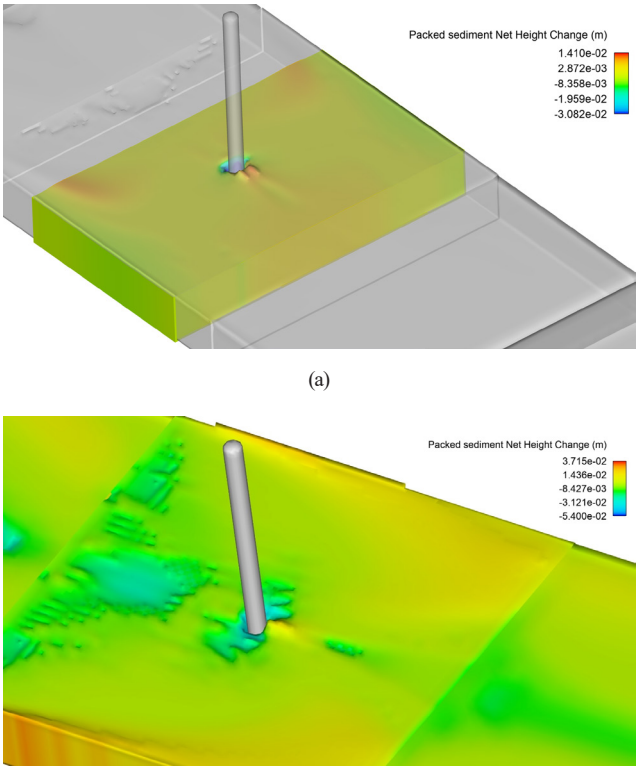

(a)

(b)

Fig. 10 Isometric views of scour development around the monopile over time: (a) Isometric view of scour analysis at 3600 s for Case 2, showing the development of scour around the monopile, (b) isometric view of scour analysis at 2800 s for Case 1 illustrating the early stages of scour development around the monopile

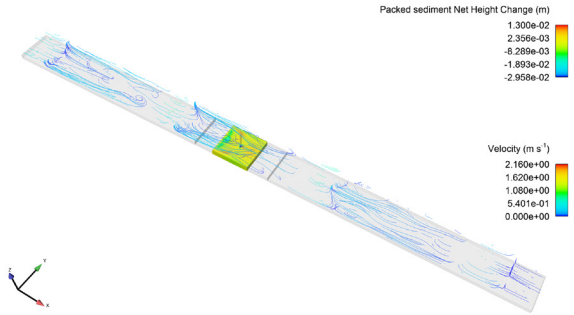

Fig. 11 Streamline visualization around the monopile, demonstrating the flow patterns and their influence on sediment transport and scour formation

three-dimensional character of the wave–structure–seabed interaction and confirms the asymmetry in scour formation.

Fig. 10(a) shows the scour depth around the monopile for Case 2 at 3600 sec, under moderate KC conditions. Sediment displacement is clearly evident, particularly on the lee side of the structure, where vortices intensify sediment transport. Fig. 10(b) presents the early stages of scour development for Case 1 at 2800 sec, illustrating limited

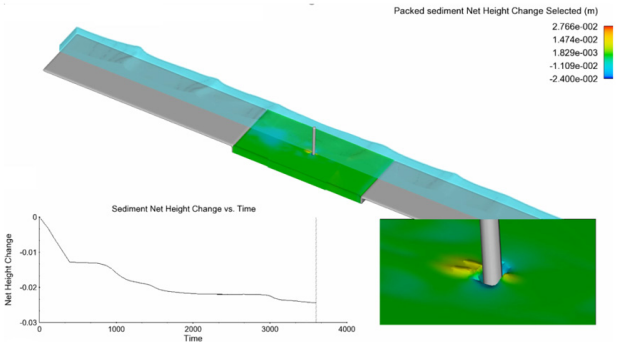

Fig. 12 Final scour depth distribution around the monopile after the simulation period, illustrating areas of maximum and minimum scour

sediment motion due to lower KC values and weaker flow dynamics. Together, these figures demonstrate how scour evolves over time as a function of hydrodynamic forcing.

To further examine flow–scour interactions, Fig. 11 displays the instantaneous streamline pattern around the monopile for KC = 14.6. The formation of flow separation and recirculation zones on the lee side is evident. These structures correspond to regions of enhanced sediment transport and local erosion. The asymmetry in streamlines reflects the influence of both inertial and drag forces at this intermediate KC regime, validating the physical realism of the simulated scour behavior. These visualizations illustrate flow separation and recirculation zones on the lee side of the monopile, suggesting the presence of asymmetric sediment transport processes that contribute to the observed scour development.

Fig. 12 presents the final scour depth distribution surrounding the monopile, highlighting both maximum and minimum scour regions. This figure captures the cumulative effect of wave forcing over the simulation duration and provides a spatially resolved depiction of the predicted scour pattern.

In the following subsections, each case from Table 1 is analyzed in detail. In all cases, the time-series plots of scour depth were extracted at a monitoring point located approximately 0.1 D downstream of the monopile, corresponding to the region of maximum erosion. The results are compared against experimental measurements and empirical estimates, allowing for a critical assessment of the model's strengths in predicting wave-induced scour and identifying potential areas for improvement.

3.1.1 Case 1

In this scenario, the numerical model was applied under a low Keulegan–Carpenter (KC) number of 8.8. Simulating scour under low KC conditions is particularly challenging due to the short flow excursion length per wave cycle, which suppresses vortex development and sediment mobilization. In such regimes, bed shear stress often remains near or below the critical Shields threshold, leading to intermittent or delayed sediment transport. Additionally, RNG k–ε turbulence models may damp out small-scale vortex structures under low-strain conditions, limiting the accuracy of near-bed flow predictions. These factors collectively contribute to conservative scour estimates in low-KC simulations.

At this KC regime and a moderate Shields parameter (θ), sediment transport remained limited, and the numerical model produced a slightly lower scour depth compared to both experimental and empirical results. This underestimation is likely associated with the reduced turbulence intensity and the challenges in representing inertia-dominated flow structures.

Fig. 13 illustrates the scour characteristics observed in the numerical simulation for a monopile with diameter D = 100 mm, wave height H_w = 17 cm, wave period T_w = 2.2 s, and particle diameter d = 0.18 mm.

Fig. 13 show the scour distribution in plan view and the variation of scour depth over time. The color gradient represents scour intensity, with darker blue indicating deeper scour zones and transitions to yellow and red indicating sediment accumulation. The visual output confirms that scour had not fully developed to its equilibrium state by the end of the simulation, suggesting a conservative numerical prediction at this time step.

The variation of scour depth over time indicates a steady increase in scour depth, with the rate of change decreasing significantly after approximately 2500 s – a behavior that suggests the approach toward an equilibrium condition. However, compared to higher KC cases, the final asymptotic plateau remains less sharply defined, likely due to the limited and slower sediment transport mechanisms inherent to inertia-dominated flow regimes. To reflect this

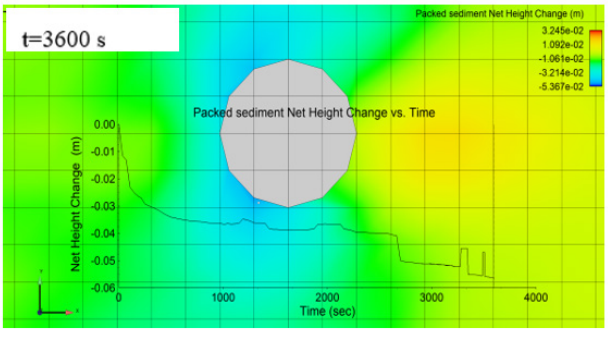

Fig. 13 Top view of scour analysis at t = 3600 s for D = 100 mm, H_w = 17 cm, wave period T_w = 2.2 s and particle diameter d = 0.18 mm

more clearly, we now interpret the Case 1 result as being near-equilibrium, rather than strictly non-equilibrium. This trend is typical for low KC inertia-dominated flows.

As summarized in Table 1, the scour depth ratio S/D observed experimentally by Sumer et al. [11] was 0.057. The empirical equation (Eq. (9)) yielded a prediction of 0.10, while the numerical model returned a slightly lower value of 0.052. Although the model underestimates the scour depth, the overall trend aligns with both the experimental and empirical results.

The observed discrepancy is likely linked to several interacting factors inherent in modeling inertia-driven scour: (i) limited bed shear exceedance of the Shields threshold under low orbital velocities, (ii) intermittent activation of the bedload transport function, and (iii) possible underprediction of turbulence intensity due to damping behavior of the turbulence closure scheme. These challenges are typical in low KC simulations, where scour initiates gradually and evolves over longer time scales. Nonetheless, the consistent pattern of gradual scour growth and the relatively small deviation from experimental values mentioned in Table 1 suggest that the numerical model captures the physical trend effectively. Further refinement of the turbulence model or transport threshold calibration could improve performance in this flow regime.

3.1.2 Case 2

In Case 2, the numerical model was evaluated under a moderate Keulegan–Carpenter (KC) number of 14.6. While the Shields parameter (θ) remained comparable to that in Case 1, the increased KC value led to enhanced sediment transport and more pronounced scour development. Under these conditions, the numerical predictions showed strong agreement with the experimental data, indicating that the combination of KC and θ effectively captures the scour process in drag-dominated regimes.

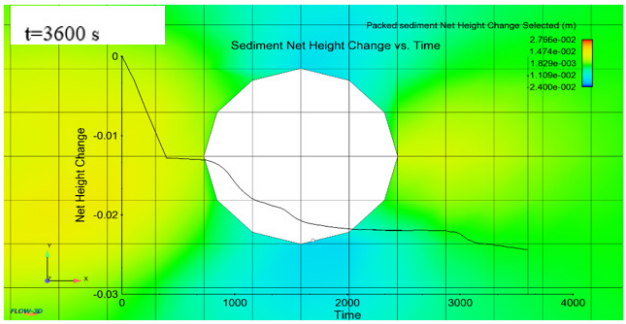

Fig. 14 Top view of scour analysis at t = 3600 s for D = 100 mm diameter, H_w = 12 cm, wave period T_w = 4.5 s and particle diameter d = 0.18 mm

Fig. 14 illustrates the scour development for a monopile with a diameter of D = 100 mm, wave height H_w = 12 cm, wave period T_w = 4.5 s, and sediment particle diameter d = 0.18 mm. Scour measurements were taken at points of maximum erosion, typically observed along the sides of the monopile. It shows a well-defined scour pattern with clear depth variations around the pile. The color gradient effectively highlights the regions of maximum and minimum scour. In contrast to Case 1, the scour has developed further and exhibits symmetry consistent with wave-induced flow separation, suggesting improved model performance in this scenario.

Fig. 14 also presents the temporal evolution of scour depth. The curve shows a steady increase in scour, with values gradually approaching a stable condition. The trend suggests that the scour is nearing the equilibrium scour depth, indicating the model's capability to simulate time-dependent scour formation under moderate KC flow regimes.

The final predicted scour depth ratio in Case 2 was S/D = 0.25, closely matching the experimental result of 0.22. Although the numerical prediction (S/D = 0.25) is qualitatively close to the experimental result (S/D = 0.22), a relative error of approximately 13.6% is observed. This level of deviation falls within the typical uncertainty bounds of sediment scour modeling and experimental variability. The empirical prediction (0.29) slightly overestimated the scour, which may be attributed to its simplified assumptions that do not fully capture the complexity of drag-dominated vortex dynamics. These findings demonstrate that the numerical model is more accurate in reproducing both the magnitude and evolution of scour under moderate wave conditions, validating its reliability in this flow regime. The improved agreement in this case may stem from the model's ability to more accurately resolve coherent vortex shedding and wake turbulence, which dominate the scour process in this KC range. The RNG k–ε turbulence closure, with its enhanced responsiveness to strain rates, appears to better capture the intensified bed shear stress fluctuations driving sediment transport.

3.1.3 Case 3

In Case 3, the numerical model was applied to simulate scour around a monopile under a higher Keulegan–Carpenter (KC) number of 24. Both the KC number and Shields parameter (θ) reached their highest values in this scenario, leading to peak sediment transport and more intense scour development. The numerical results closely

matched the experimental observations, while the empirical prediction tended to slightly overestimate the scour depth.

Fig. 15 presents the simulation results for a monopile with a diameter of D = 100 mm, wave height H_w = 22 cm, wave period T_w = 4.5 s, and sediment particle diameter d = 0.18 mm. Scour was monitored at probe points placed near areas of maximum expected erosion, typically along the sides of the pile where flow separation and vortex activity are most intense.

It displays a well-developed scour profile with significant depth variations. The color gradient clearly indicates deeper scour zones near the pile, consistent with the presence of stronger wave-induced flow and vortex generation. These results demonstrate the model's ability to reproduce the spatial distribution and intensity of scour under high KC conditions.

Fig. 15 also shows the temporal evolution of scour depth. The results reveal an initially rapid increase in scour, followed by a gradual approach toward an equilibrium scour depth. This trend is typical of drag-dominated flow regimes, where intensified vortex shedding promotes rapid sediment removal and earlier stabilization of scour depth. After the equilibrium stage is reached ($t \approx 1000$ s), minor oscillations are observed in the time-series plot (Fig. 15). These fluctuations may be associated with localized vortex shedding and sediment recirculation, which could cause alternating erosion and slight backfilling near the monopile. While not quantitatively examined in this study, such behavior is consistent with the unsteady nature of scour development in drag-dominated flows.

In this case, the numerical model predicted a dimensionless scour depth of S/D = 0.30, in close agreement with the experimental value of 0.31. The empirical formula (Eq. (8)) yielded a slightly higher value of 0.54, indicating an overestimation in this high-energy regime. These findings suggest

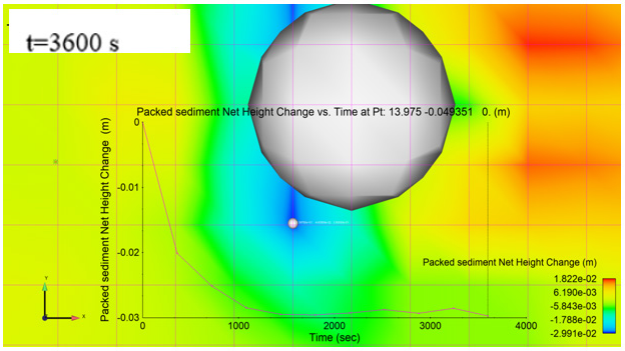

Fig. 15 Top view of scour analysis at t = 3600 s for D = 100 mm, H_w = 22 cm, wave period T_w = 4.5 s and particle diameter d = 0.18 mm

that while the empirical approach provides a conservative estimate, the numerical model more accurately captures the underlying physics of scour under high KC conditions.

The strong agreement between numerical and experimental results in Case 3 underscores the model's reliability in simulating wave-induced scour under high KC conditions, where the flow regime is predominantly drag-dominated and characterized by stronger vortex shedding and intensified lee-wake turbulence. This suggests that the employed turbulence and sediment transport models are well-suited to capture the complex flow–seabed interactions that govern scour evolution in such energetic environments.

3.2 Validation with experimental and empirical results

To facilitate a clearer evaluation of the model performance, this section separately compares the numerical results from Section 3.1 with the available experimental and empirical data. Each validation case (Cases 1–3) is directly linked to its corresponding simulation results discussed earlier. In this section, the numerical simulation results are validated through comparisons with experimental data from Sumer et al. [11] and empirical formulations, particularly the expression in Eq. (8). These comparisons evaluate the model's capability to predict both the magnitude and temporal development of scour depth under wave-induced flow conditions. The validation is performed over a range of Keulegan–Carpenter (KC) numbers, allowing the influence of flow regime on model accuracy to be assessed. The analysis focuses not only on the final scour depths but also on the dimensionless time evolution, which provides further insight into the progression and rate of scour development across different flow intensities.

The temporal evolution of scour was assessed by analyzing the dimensionless scour depth S/D as a function of the dimensionless time scale T^*, which is a critical parameter for characterizing the rate of scour development under wave action. This parameter incorporates both sediment properties and hydrodynamic forcing and is defined as:

$$T^* = \frac{\sqrt{g\left(s1-\right)d^3}}{D^2}t \tag{9}$$

where t is time, g is the gravitational acceleration, ρ_s and ρ are sediment and fluid densities, d is the median grain diameter, and D is the pile diameter. This normalization enables a consistent comparison between numerical and experimental results across different flow regimes and KC numbers.

In Case 1 (KC = 8.8), the numerical model shows a progressive increase in scour depth over time, eventually converging

to the final equilibrium value reported in the experimental study by Sumer et al. [11], as illustrated in Fig. 16. It should be noted that the experimental data provides only this final scour depth; no temporal data regarding scour initiation or its time evolution is available. Therefore, any assessment of scour initiation timing or early-phase behavior is based solely on numerical results and cannot be directly compared to experimental measurements.

The relatively slow scour development observed in the simulation can be attributed to the nature of the inertia-dominated flow regime at low KC values, where fluid excursion per wave cycle is limited and vortex generation is weak. These conditions delay the onset of sediment mobilization, making the scour process more gradual and challenging to capture with high fidelity in numerical models.

Additionally, factors such as numerical diffusivity, near-bed mesh resolution, and sediment transport modeling – particularly the use of threshold-based bedload formulations (e.g., critical Shields parameter) – may lead to delayed sediment response in the early stages of the simulation.

While the earlier onset of scour observed in similar laboratory conditions may be influenced by unmodeled factors such as boundary roughness, sediment compaction, or wave flume effects, the numerical model nonetheless captures the long-term trend and asymptotic behavior of scour development consistent with the experimental final value.

In contrast to the low-KC case, model performance improves significantly in Case 2 (KC = 14.6), where the flow regime becomes drag-dominated. These conditions enhance vortex shedding and sediment mobilization, which are more effectively resolved by the numerical scheme. As shown in Fig. 6, the model accurately reproduces both the trend and equilibrium scour depth observed in the experimental time-series data. The agreement is particularly strong in the intermediate and later stages of scour development, indicating that the RNG k–ε turbulence closure and sediment transport formulation are well-suited to capturing the relevant physical processes in this flow regime.

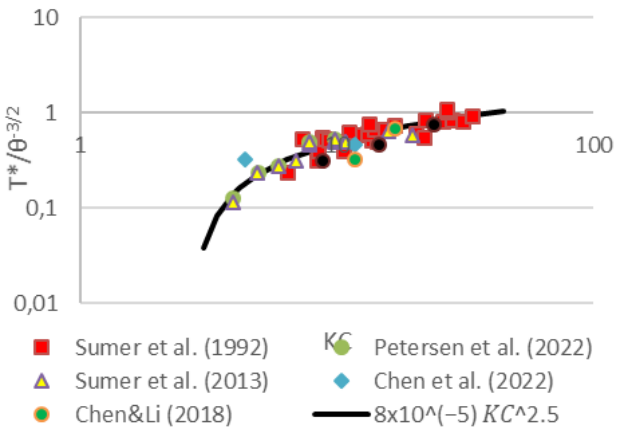

Fig. 16 Comparison of $T^*/\theta^{-3/2}$ across varying KC numbers between the numerical results of this study (black circle) and the empirical data from Larsen and Fuhrman [22]

For Case 3 (KC = 24), the scour process accelerates under intense wave forcing, driven by dominant drag forces and energetic vortex shedding. As shown in Fig. 7, the numerical model rapidly reaches a scour depth that aligns closely with the final experimental value reported by Sumer et al. [11]. Because experimental time-series data for this case are not available, only the final equilibrium depth can be used for validation. The model's slight early overprediction may stem from enhanced local shear effects induced by mesh resolution and turbulence closure, yet the predicted scour stabilizes at a value consistent with the benchmark data. This result further supports the model's capability in resolving highly energetic, drag-dominated scour regimes.

To further evaluate the reliability of the model in predicting scour development timescales, the results were compared with the empirical relation proposed by Larsen and Fuhrman [22], given by: $T^* = 8 \times 10 - 5KC^{2.5}$. This expression provides a reference for the expected dimensionless scour time T^* as a function of the Keulegan–Carpenter number and serves as a useful benchmark for validating the temporal dynamics of the numerical simulations. In this study, the numerically obtained values of $T^*/\theta^{-3/2}$ were plotted against KC and compared to the empirical trend, as shown in Fig. 16.

The results demonstrate that the numerical predictions follow the empirical curve closely across all KC values considered, particularly in the drag-dominated regime (KC > 10). This agreement confirms that the model not only captures the final scour depth accurately, but also resolves the temporal progression of scour in a physically consistent manner, further validating its predictive capability.

Overall, the validation results confirm that the numerical model provides reliable predictions of both equilibrium scour depths and associated timescales across a broad range of Keulegan–Carpenter numbers. The model demonstrates increasing accuracy with higher KC values, where flow becomes more drag-dominated and sediment transport is driven by well-resolved vortex structures and recirculation zones. While some underestimation is observed in low-KC, inertia-dominated conditions – primarily due to limitations in resolving weak vortex shedding and delayed sediment initiation – the model consistently

captures the overall trend, magnitude, and progression of scour. Its ability to reproduce experimental observations and follow empirical scaling laws underscores its robustness and applicability for practical offshore engineering scenarios involving wave-induced scour.

3.3 Influence of cylinder grouping on scour patterns

The influence of cylinder grouping on scour development was investigated through additional numerical simulations using two spacing configurations: $G/D = 1$ and $G/D = 2$, where G is the center-to-center distance between the monopiles and D is the pile diameter. The Keulegan–Carpenter number was fixed at KC = 13, and other simulation parameters – such as wave period (4.5 s), wave height, water depth, and sediment properties – were kept consistent with the single-cylinder conditions reported in experimental studies. Fig. 17 presents an overview of the numerical domain and the spatial arrangement of the grouped monopiles.

The interpretations regarding hydrodynamic interactions and flow effects in the grouped monopile configurations are derived from sediment transport patterns and scour profiles illustrated in Figs. 18 and 19. While direct flow field or vorticity visualizations are not presented, these sediment-based observations provide valuable indirect insight into the local flow dynamics and scour mechanisms.

In the case of G/D = 1, the cylinders are closely spaced, resulting in strong hydrodynamic interaction between them. Figs. 18(a) and 18(b) illustrate sediment transport and scour profiles indicating that the region between the two cylinders has limited sediment movement and relatively stable bed elevation, which suggests reduced flow velocity and possible vortex effects in that zone. However, sediment and scour profiles near the downstream cylinder indicate stronger local sediment mobilization, which may be attributed to increased turbulence and flow reattachment. The maximum scour depth in this configuration was approximately $S/D \approx 0.28$, which slightly exceeds the experimentally reported equilibrium scour depth of $S/D \approx 0.26$ for a single pile at the same KC number [11], indicating a mild amplification effect induced by grouping.

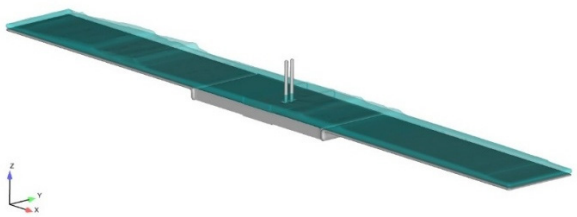

Fig. 17 Numerical domain overview showing the flow field and cylinder arrangement

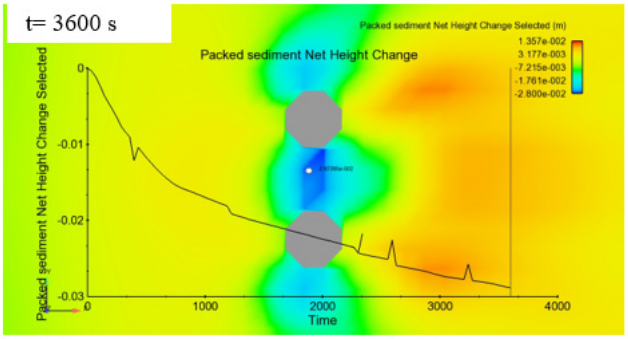

(a)

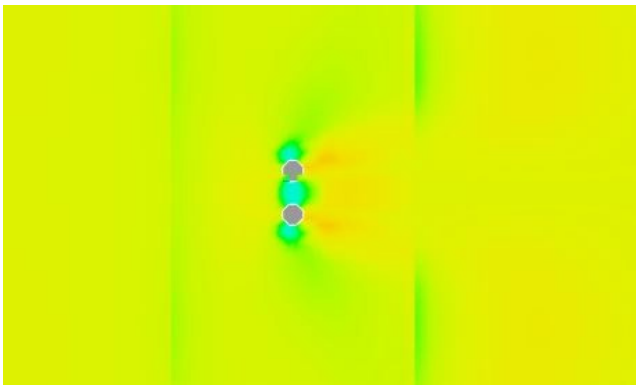

(b)

Fig. 18 Scour and sediment transport patterns for the first set of simulations with $G/D = 1$: (a) Packed sediment net height change for cylinders with spacing ratio $G/D = 1$; (b) Scour profile near downstream cylinder for $G/D = 1$.

When the spacing is increased to $G/D = 2$, each cylinder interacts more independently with the incoming wave field, and the flow interference between them is reduced. As illustrated in Figs. 19(a) and 19(b), the scour patterns become more symmetric and less severe. In this configuration, the maximum downstream scour depth was approximately $S/D \approx 0.18$, which is significantly lower than the single-cylinder benchmark. This reduction highlights the sheltering influence of the upstream pile and the stabilizing effect of increased spacing.

These findings underscore the critical role of pile spacing in shaping local scour characteristics. A smaller spacing ratio ($G/D = 1$) creates a zone of hydrodynamic shielding between the piles, reducing sediment removal in the intermediate region but potentially intensifying scour downstream due to confined flow reattachment. In contrast, a larger spacing ratio ($G/D = 2$) promotes more balanced and independent scour patterns, yet the overall scour intensity near each pile remains lower.

It is acknowledged that this study focuses exclusively on a two-pile tandem arrangement under fixed wave conditions, and the conclusions drawn are limited to this

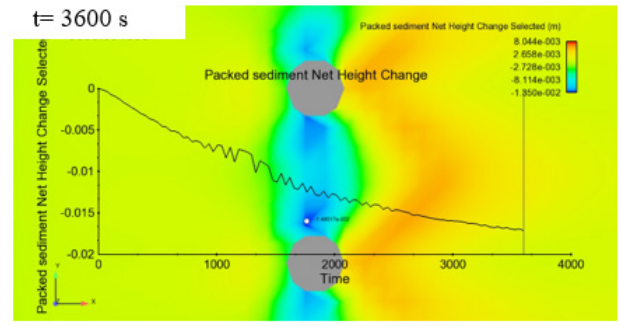

(a)

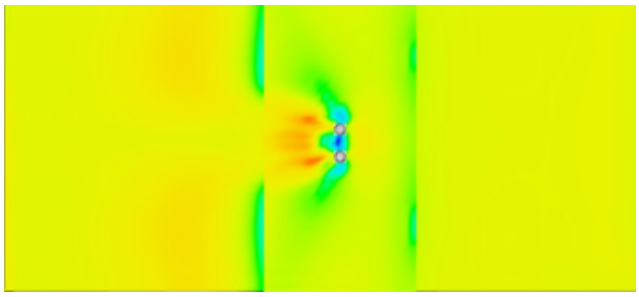

(b)

Fig. 19 Scour and sediment transport patterns for the second set of simulations with $G/D = 2$: (a) Packed sediment net height change for cylinders with spacing ratio $G/D = 2$; (b) Scour profile near downstream cylinder for $G/D = 2$.

specific configuration. Nevertheless, the results provide valuable insight into local flow interaction mechanisms and spacing effects within the context of closely spaced monopile foundations. These insights highlight the importance of considering group effects in the design and layout of offshore monopile foundations, particularly for environments characterized by oscillatory wave forcing.

4 Conclusions

This study presented a numerical investigation of wave-induced scour around slender monopiles subjected to varying Keulegan–Carpenter (KC) numbers, using a validated computational fluid dynamics (CFD) model. The results showed that higher KC values lead to intensified vortex shedding and increased sediment transport, resulting in more severe scour depths. Conversely, lower KC values were associated with gradual scour development due to limited flow excursion and weaker vortex activity. The numerical predictions exhibited good agreement with experimental data from Sumer et al. [11], supporting the model's capability to replicate dominant scour mechanisms under regular wave forcing.

In addition to single-cylinder cases, grouped monopile configurations with spacing ratios of $G/D = 1$ and $G/D = 2$ were simulated to examine the effect of pile arrangement at KC = 13. The results showed that the closer spacing ($G/D = 1$) led to deeper scour near the downstream pile, with $S/D \approx 0.28$, whereas wider spacing ($G/D = 2$) resulted in a milder response, with $S/D \approx 0.18$. These findings reflect stronger flow acceleration and vortex-induced turbulence within the narrow gap, contrary to the commonly assumed sheltering behavior. However, it is important to note that these interpretations are primarily based on sediment transport and scour profiles, without direct flow field or turbulence measurements, underscoring the need for case-specific assessment of vortex dynamics, especially in tandem arrangements under oscillatory flow.

The CFD model used in this study demonstrated sensitivity to spacing configurations and captured key features of sediment response in both isolated and grouped scenarios. Although no new design charts or parametric formulas were developed, the simulation results offer a reference for validating future experimental studies and numerical frameworks focused on offshore foundation scour.

Finally, while the current analysis was limited to regular wave input and uniform sediment, it provides a basis for further model development. Incorporating additional complexities such as irregular wave spectra, combined wave–current conditions, and variable seabed characteristics would improve applicability to real-world engineering problems. These limitations highlight the need for caution in generalizing the present findings beyond the specific configurations examined. Despite these limitations, the present findings contribute to ongoing efforts to better understand scour progression around monopile structures, particularly in clustered or closely spaced layouts commonly found in offshore wind farm development.

Nomenclature

S	Scour depth
D	Diameter of the monopile
G	Gap between cylinders
KC	Keulegan-Carpenter number, related to wave-induced forces
T	Wave period
H_w	Wave height
U_m	Orbital velocity
Θ	Shields parameter
θ_{cr}	Critical Shields parameter (threshold for sediment motion)
T^*	Dimensionless time
Φ	Dimensionless sediment transport rate

B	Empirical coefficient in the sediment transport calculation
q_b	Volumetric sediment transport rate
g	Gravitational acceleration
ρ_s	Sediment density
ρ	Fluid density
d_s	Sediment particle diameter
v	Kinematic viscosity of the fluid
P	Pressure
S_{ij}	Mean strain rate tensor
v_t	Turbulent viscosity
u_i	Velocity component in the i-th direction
δ_{ij}	Kronecker delta
u	Fluid velocity vector
C_s	Sediment concentration

References

[1] Prendergast, L. J., Gavin, K., Doherty, P. "An investigation into the effect of scour on the natural frequency of an offshore wind turbine", Ocean Engineering, 101, pp. 1–11, 2015. https://doi.org/10.1016/j.oceaneng.2015.04.017

[2] Zhang, J., Issa, F., Sun, K. "A glance at offshore wind turbine foundation structures", Brodogradnja, 67(2), pp. 101–113, 2016. https://doi.org/10.21278/brod67207

[3] Najafzadeh, M., Saberi-Movahed, F. "GMDH-GEP to predict free span expansion rates below pipelines under waves", Marine Georesources & Geotechnology, 37(3), pp. 375–392, 2019. https://doi.org/10.1080/1064119x.2018.1443355

[4] Ehteram, M., Meymand, A. M. "Numerical modeling of scour depth at side piers of the bridge", Journal of Computational and Applied Mathematics, 280, pp. 68–79, 2015. https://doi.org/10.1016/j.cam.2014.11.039

[5] Najafzadeh, M., Oliveto, G. "More reliable predictions of clear-water scour depth at pile groups by robust artificial intelligence techniques while preserving physical consistency", Soft Computing, 25(7), pp. 5723–5746, 2021. https://doi.org/10.1007/s00500-020-05567-3

[6] Ye, H., Fan, Y., Bai, W., Jiang, C. "Experimental study of coupling response characteristics of offshore monopiles, seabed, and waves in various sea conditions", Scientific Reports, 14(1), 28560, 2024. https://doi.org/10.1038/s41598-024-79858-2

[7] Guo, R., Lo, P. H.-Y. "Numerical investigation on solitary wave interaction with a vertical cylinder over a viscous mud bed", Water, 14(7), 1135, 2022. https://doi.org/10.3390/w14071135

[8] Xu, C., Huang, Z. "An experimental study of characteristics of solitary-wave-induced scour around a pile breakwater with a discussion on effects of the distance between piles", Journal of Earthquake and Tsunami, 16(3), 2240002, 2022. https://doi.org/10.1142/S1793431122400024

[9] Zhang, S., Li, B., Ma, H. "Numerical investigation of scour around the monopile using CFD-DEM coupling method", Coastal Engineering, 183, 104334, 2023. https://doi.org/10.1016/j.coastaleng.2023.104334

[10] Ma, H., Zhang, S., Li, B., Huang, W. "Local scour around the monopile based on the CFD-DEM method: Experimental and numerical study", Computers and Geotechnics, 168, 106117, 2024. https://doi.org/10.1016/j.compgeo.2024.106117

[11] Sumer, B. M., Fredsøe, J., Christiansen, N. "Scour around a vertical pile in waves", Journal of Waterway, Port, Coastal, and Ocean Engineering, 118(1), pp. 15–31, 1992. https://doi.org/10.1061/(ASCE)0733-950X(1992)118:1(15)

[12] Whitehouse, R. "Scour at Marine Structures: A Manual for Practical Applications", Emerald Publishing Limited, 1998. ISBN 978-0-7277-3857-8 http://doi.org/10.1680/sams.26551

[13] Melville, B. W., Coleman, S. E. "Bridge Scour", Water Resources Publications, 2000. ISBN 978-1-887201-18-6

[14] Sumer, B. M., Fredsøe, J. "The Mechanics of Scour in the Marine Environment", World Scientific, 2002. ISBN 978-981-3105-95-9 https://doi.org/10.1142/4942

[15] Fowai, I., Zhang, J., Sun, K., Wang, B. "Structural analysis of jacket foundations for offshore wind turbines in transitional water", Brodogradnja, 72(1), pp. 109–124, 2021. https://doi.org/10.21278/brod72106

[16] Farooq, R., Ghumman, A. R., Tariq, M. A. U. R., Ahmed, A., Jadoon, K. Z. "Optimal octagonal hooked collar countermeasure to reduce scour around a single bridge pier", Periodica Polytechnica Civil Engineering, 64(4), pp. 1026–1037, 2020. https://doi.org/10.3311/PPci.15966

[17] Petersen, T. U., Sumer, B. M., Fredsøe, J. "Time scale of scour around a pile in combined waves and current", In: ICSE-6: 6th International Conference on Scour and Erosion, Paris, France, 2012.

[18] Zhang, B., Li, J., Liu, W., Zhang, H., Shi, P., Fu, X. "Experimental study on dynamic characteristics of a monopile foundation based on local scour in combined waves and current", Ocean Engineering, 266, 113003, 2022. https://doi.org/10.1016/j.oceaneng.2022.113003

[19] Sumer, B. M., Petersen, T. U., Lucatelli, L., Fredsøe, J., Musumeci, R. E., Foti, E. "Backfilling of a scour hole around a pile in waves and current", Journal of Waterway, Port, Coastal, and Ocean Engineering, 139(1), pp. 9–23, 2013. https://doi.org/10.1061/(asce)ww.1943-5460.0000161

[20] Chen, J., Li, Y. "Experimental study of local scour around a vertical cylinder under wave-only and combined wave-current conditions in a large-scale flume", Journal of Hydraulic Engineering, 144(9), 04018058, 2018. https://doi.org/10.1061/(asce)hy.1943-7900.0001502

[21] Chen, S. G., Gong, E., Zhao, X., Arikawa, T., Chen, X. "Large-scale experimental study on scour around offshore wind monopiles under irregular waves", Water Science and Engineering, 15(1), pp. 40–46, 2022. https://doi.org/10.1016/j.wse.2021.12.003

[22] Larsen, P., Fuhrman, D. R. "Re-parameterization of equilibrium scour depths and time scales for monopiles", Coastal Engineering, 185, 104356, 2023. https://doi.org/10.1016/j.coastaleng.2023.104356

[23] Gumgum, F., Guney, M. S. "Time Dependent Live-bed Scour Around Circular Piers under Flood Waves", Periodica Polytechnica Civil Engineering, 64(1), pp. 65–72, 2020. https://doi.org/10.3311/PPci.14664

[24] Lai, Y. G., Liu, X. F., Bombardelli, F. A., Song, Y. "Three-dimensional numerical modeling of local scour: A state-of-the-art review and perspective", Journal of Hydraulic Engineering, 148(11), 03122002, 2022. https://doi.org/10.1061/(asce)hy.1943-7900.0002019

[25] Zhao, M., Vaidya, S., Zhang, Q., Cheng, L. "Local scour around two pipelines in tandem in steady current", Coastal Engineering, 98, pp. 1–15, 2015. https://doi.org/10.1016/j.coastaleng.2015.01.001

[26] Zhao, M., Teng, B., Cheng, L. "Numerical simulation of wave-induced local scour around a large cylinder", Coastal Engineering Journal, 46(3), pp. 291–314, 2004. https://doi.org/10.1142/s0578563404001075

[27] Hirt, C. W., Nichols, B. D. "Volume of Fluid (VOF) method for the dynamics of free boundaries", Journal of Computational Physics, 39(1), pp. 201–225, 1981. https://doi.org/10.1016/0021-9991(81)90145-5

[28] Ferziger, J. H., Perić, M. "Computational Methods for Fluid Dynamics", Springer Berlin, Heidelberg, 2002. ISBN 978-3-642-56026-2 https://doi.org/10.1007/978-3-642-56026-2

[29] Yakhot, V., Orszag, S. A. "Renormalization group analysis of turbulence. I. Basic theory", Journal of Scientific Computing, 1(1), pp. 3–51, 1986. https://doi.org/10.1007/BF01061452

[30] Omara, H., Tawfik, A. "Numerical investigation of scour around bridge piers", IOP Conference Series: Earth and Environmental Science, 151, 012013, 2018. https://doi.org/10.1088/1755-1315/151/1/012013

[31] Jalal, H. K., Hassan, W. H. "Numerical Investigation of Local Scour Around Bridge Piers Using FLOW-3D", IOP Conference Series: Materials Science and Engineering, 745, 012150, 2020. https://doi.org/10.1088/1757-899X/745/1/012150